Food Chemistry 370 (2022) 131292

Contents lists available at ScienceDirect

Food Chemistry

journal homepage: www.elsevier.com/locate/foodchem

Unravelling discolouration caused by iron-flavonoid interactions: Complexation, oxidation, and formation of networks

Judith Bijlsma [a], Wouter J.C. de Bruijn [a], Krassimir P. Velikov [b,c,d], Jean-Paul Vincken [a,*]

[a] Laboratory of Food Chemistry, Wageningen University & Research, Bornse Weilanden 9, P.O. Box 17, 6700 AA Wageningen, the Netherlands
[b] Unilever Innovation Centre B.V. Bronland 14, 6708 WH Wageningen, the Netherlands
[c] Institute of Physics, University of Amsterdam, Science Park 904, 1098 XH Amsterdam, the Netherlands
[d] Soft Condensed Matter, Debye Institute for Nanomaterials Science, Utrecht University, Princetonplein 5, 3584 CC Utrecht, the Netherlands

ARTICLE INFO

Keywords:
Ferrous
Ferric
Polyphenol
Metal chelation
Auto-oxidation
Ligand-to-metal charge transfer

ABSTRACT

Iron-flavonoid interactions in iron-fortified foods lead to undesirable discolouration. This study aimed to investigate iron-mediated complexation, oxidation, and resulting discolouration of flavonoids by spectrophotometric and mass spectrometric techniques. At pH 6.5, iron complexation to the 3–4 or 4–5 site instantly resulted in bathochromic shifting of the $\pi \rightarrow \pi^*$ transition bands, and complexation to the 3'-4' site (*i.e.* catechol moiety) induced a $\pi \rightarrow d_\pi$ transition band. Over time, iron-mediated oxidative degradation and coupling reactions led to the formation of hydroxybenzoic acid derivatives and dehydrodimers, respectively resulting in a decrease or increase in discolouration. Additionally, we employed XRD, SEM, and TEM to reveal the formation of insoluble black metal-phenolic networks (MPNs). This integrated study on iron-mediated complexation and oxidation of flavonoids showed that the presence of the *C2–C3* double bond in combination with the catechol moiety and either the 4-carbonyl or 3-hydroxyl increased the intensity of discolouration, extent of oxidation, and formation of MPNs.

1. Introduction

Food fortified with iron can effectively reduce the global prevalence of iron deficiency (Allen, De Benoist, Dary, & Hurrell, 2006). However, when food is fortified with iron, its colour and iron bioavailability can be compromised by the reactivity of the iron ion with flavonoids (Habeych, van Kogelenberg, Sagalowicz, Michel, & Galaffu, 2016). Flavonoids are secondary plant metabolites that are ubiquitous in vegetables, herbs, and fruits. These compounds affect food colour and flavour, and possess a broad range of biological activities. The class of flavonoids includes several subclasses that share the same flavan (2-phenylchromen-4-one) backbone but possess different structural features based on the degree of oxidation of the pyran C-ring (Fig. 1A).

Hydroxyl and carbonyl groups on the flavan backbone can coordinate metal ions to form stable complexes. Flavonoids possess several structural moieties that can bind metal ions via coordinate bonds: (i) the 3-hydroxy-4-ketone moiety in the C-ring (3–4 site), (ii) 5-hydroxy-4-ketone moiety (4–5 site), and (iii) the 3'-4'-dihydroxy moiety located in the B-ring (3'-4' site) (Fig. 1B) (Uivarosi, Munteanu, Sharma, & Singh Tuli, 2019). The stoichiometry of iron-flavonoid complexes (*e.g.* 1:1, 1:2, and 2:1) and preferred iron-binding sites are dependent on the solvent, the pH of the sample, iron source, and flavonoid structure (Kasprzak, Erxleben, & Ochocki, 2015). Ferrous sulphate ($FeSO_4$) is used as iron source, since it is the most common iron fortificant in food owing to affordability, bioavailability, and (regulatory) acceptance by authorities and consumers (Allen et al., 2006). Complexation of flavonoids to Fe^{2+} is followed by fast auto-oxidation to Fe^{3+} because phenolic ligands stabilise Fe^{3+} over Fe^{2+} (Perron & Brumaghim, 2009).

Complexation of metals by flavonoids changes the flavonoids' absorbance spectra, resulting in a bathochromic (red) shift (Kasprzak et al., 2015). Complexation of Fe^{3+} to the catechol moiety (*i.e.* 3'-4' site in flavonoids) causes intense off-colour development resulting from ligand-to-metal charge transfer (LMCT) phenomena, also referred to as $\pi \rightarrow d_\pi$ transitions (Elhabiri, Carrër, Marmolle, & Traboulsi, 2007; Mellican, Li, Mehansho, & Nielsen, 2003). Typically, these $\pi \rightarrow d_\pi$ transitions result in a bathochromic shift of the absorbance and formation of a broad absorbance band ranging from 380 to 800 nm. Besides this, bathochromic shifting of the $\pi \rightarrow \pi^*$ transitions to around 425 nm has also been reported for flavonoids due to an increase in the size of the conjugated system upon Fe^{3+} complexation (Guo et al., 2007; Ren,

* Corresponding author.
E-mail address: jean-paul.vincken@wur.nl (J.-P. Vincken).

https://doi.org/10.1016/j.foodchem.2021.131292
Received 13 July 2021; Received in revised form 27 September 2021; Accepted 29 September 2021
Available online 2 October 2021

Meng, Lekka, & Kaxiras, 2008). Such a shift of $\pi \rightarrow \pi^*$ transitions was also reported for flavonoids, that contained solely a 4–5 binding site (Dowling, Regan, & Hughes, 2010). Iron complexation to flavonoids that contain solely a 3–4 site has hitherto not been reported and its effects on absorbance spectra, including the underlying transition mechanisms, are yet unknown. Thus far, it remains unclear whether the shift in absorbance upon complexation of iron to either one or all three of the different binding sites of flavonoids is due to LMCT ($\pi \rightarrow d_\pi$ transitions), increased size of the conjugated system ($\pi \rightarrow \pi^*$ transitions), or a combination thereof (Kasprzak et al., 2015).

Coordinate bond formation between Fe^{3+} and flavonoids can be followed by a redox reaction, via electron transfer (ET) from the flavonoid to iron (Ryan & Hynes, 2008). In this process, the complexed Fe^{3+} is reduced to Fe^{2+} and the flavonoid is thereby oxidised to a semiquinone-type radical, and a quinone upon a second ET (Fig. 1C). Subsequent reactions of the flavonoid quinones yield a plethora of products arising from degradation and oxidative coupling. Extension of the conjugated system of the flavonoid upon oxidative coupling contributes to browning (Tan, de Bruijn, van Zadelhoff, Lin, & Vincken, 2020). Additionally, the resulting degradation and oxidative coupling products may form complexes with iron, and thereby further affect the colour.

Iron-mediated complexation and oxidation are affected by the structural features of flavonoids as previously demonstrated by the structure–activity relationships established for iron complexation and radical scavenging, both measures of the antioxidant activity of flavonoids. Flavonoids possessing the catechol or pyrogallol moieties are generally stronger antioxidants because of the stability constants for binding of the 3'-4' site to iron (Mladěnka et al., 2011; Perron & Brumaghim, 2009). Furthermore, the presence of the 3-OH and/or the 5-OH in combination with the *C*4 keto group and the *C*2–*C*3 double bond is also associated with Fe^{3+}-complexation and reported to confer increased Fe^{3+}-reducing capacity (Khokhar & Owusu Apenten, 2003; Mira et al., 2002). The Fe^{3+}-mediated oxidation of catechol and other phenolics at neutral pH is reported to be slow (Bijlsma et al., 2020; Hajji, Nkhili, Tomao, & Dangles, 2006; Nkhili, Loonis, Mihai, El Hajji, & Dangles, 2014). However, in these reports, the interaction between Fe^{3+} and phenolics was usually measured over a short timespan (*e.g.* 1 h). Longer-term effects should be considered to more realistically mimic the iron-flavonoid interactions that can take place during food processing, storage, and preparation.

The aforementioned studies have focussed primarily on separately assessing either iron-mediated complexation or oxidation of flavonoids, and not the combined and interconnected effect of these two interactions on discolouration. Therefore, we aimed to comprehensively investigate the combination of iron-mediated complexation and oxidation on the discolouration of a set of structurally different flavonoids. Ten different flavonoids were incubated with iron ($FeSO_4$) and the influence of structural features on discolouration were assessed. The contribution of complexation and oxidation to discolouration was elucidated via spectrophotometric and mass spectrometric techniques. Because complexation is known to affect iron bioavailability, the proportion of water soluble iron at pH 6.5 was investigated as a first indicator for iron bio-accessibility (Wienk, Marx, & Beynen, 1999) in presence of our broad set of flavonoids.

We hypothesised that (i) fast discolouration is caused by iron-flavonoid complexation; (ii) oxidation of flavonoids over time affects discolouration; (iii) structural features of the flavonoid, specifically the hydroxylation of the B-ring, the *C*2–*C*3 double bond, and the 3-hydroxy-4-keto moiety, and combinations thereof contribute to complexation and oxidation; and (iv) that the catechol moiety on the B-ring is prerequisite for LMCT. To the best of the authors' knowledge, this is the first integrated study investigating the combined effect of iron-mediated complexation and oxidation on the discolouration of a structurally diverse set of flavonoids.

2. Materials and methods

2.1. Chemicals

Quercetin hydrate (≥95 %), 4-hydroxybenzoic acid (≥99 %), 3,4,5-trihydroxybenzoic acid (≥98 %), iron(II) sulphate heptahydrate (≥99 %), and 3-(2-pyridyl)-5,6-diphenyl-1,2,4-triazine-p,p'-disulfonic acid monosodium salt hydrate (≥97 %; ferrozine) were obtained from Sigma Aldrich (St. Louis, MO, USA). Myricetin (≥97 %), naringenin (≥93 %),

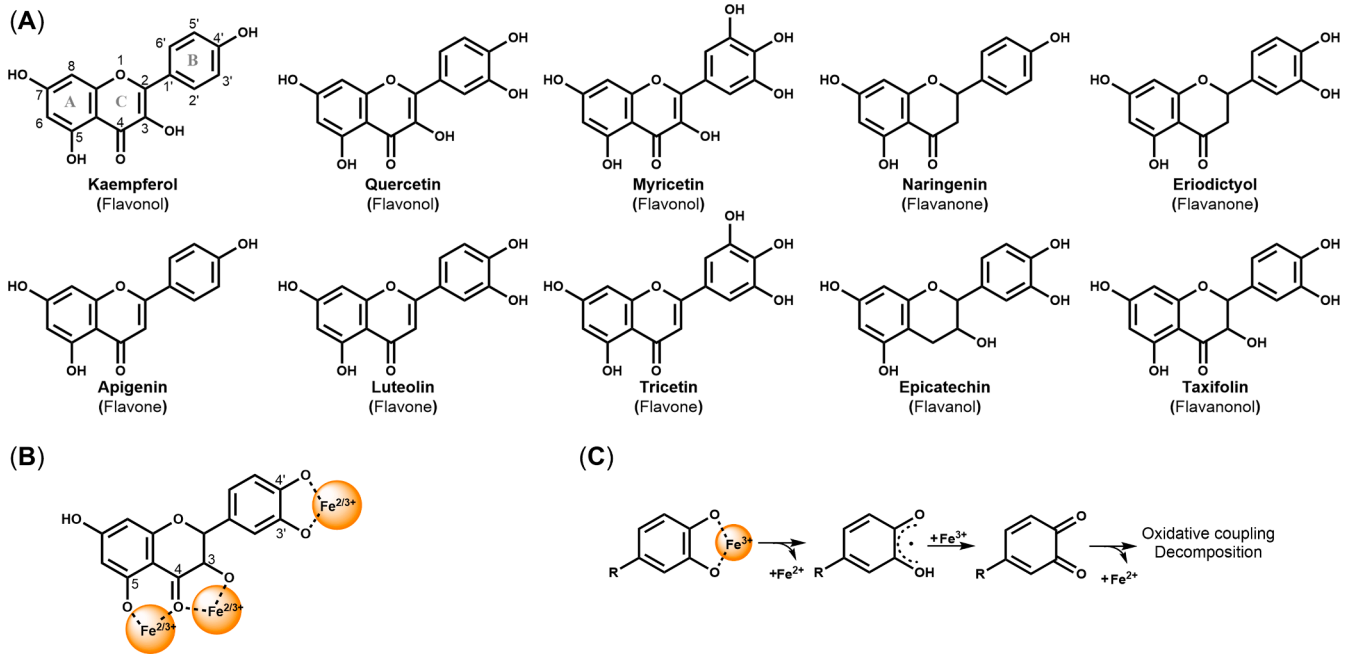

Fig. 1. (A) Overview of the dietary flavonoids investigated in this study, the corresponding flavonoid subclass is indicated between brackets; (B) possible binding sites of iron ions (in ferrous or ferric state) on flavonoids; (C) oxidation of the flavonoid 3'-4' site to a semiquinone-type radical and eventually to a quinone in presence of ferric iron.

epicatechin (≥97 %), 3,4-dihydroxybenzoic acid (≥98 %) and 2,4,6-trihydroxybenzoic acid (≥98 %) were purchased from TCI Europe NV (Zwijndrecht, Belgium). Kaempferol (≥99 %), luteolin (≥98 %), eriodictyol (≥99 %), and taxifolin (≥98 %) were purchased from Extrasynthese (Genay, France), apigenin (≥98 %) from Indofine Chemical Company (Hillsborough, NJ, USA), and tricetin (≥95 %) from Specs (Delft, The Netherlands). Ascorbic acid (≥99 %) was obtained from VWR International (Radnor, PA, USA). Dimethylsulfoxide (DMSO) was obtained from Merck Millipore (Billerica, MA, USA). ULC-MS grade acetonitrile (ACN) and water, both containing 0.1 % (*v/v*) formic acid (FA) were purchased from Biosolve (Valkenswaard, the Netherlands). Water for other purposes than UHPLC was prepared using a Milli-Q water purification system (Merck Millipore, Billerica, MA, USA).

2.2. Incubation of flavonoids with or without iron

Stock solutions of each flavonoid were made by dissolving them in DMSO to a 20 mM concentration. Subsequently, each flavonoid stock solution was diluted either in water (flavonoid blank; final concentration flavonoid 1 mM; pH 6.0–7.5) or in a freshly prepared $FeSO_4$ solution (iron-flavonoid; final concentration flavonoid 1 mM; final concentration Fe^{2+} 1 mM; pH 4.5–5.0), for the iron blank a solution of 1 mM $FeSO_4$ was prepared (pH 5.0). The final volume of all samples was 10 mL, containing 5 % (*v/v*) DMSO. An aliquot of 0.5 mL was taken from the sample immediately after adding the flavonoid ($t_{0'}$). Subsequently, each sample was adjusted to pH 6.5 by using a pH-stat device (Metrohm, Herisau, Switzerland), and during the experiment the pH was maintained at 6.5 with automated titration using 0.05 M HCl and 0.05 M NaOH. This approach of maintaining pH with concentrated HCl and NaOH was chosen as buffer compounds can cause interference with complexation and oxidation reactions (Andjelković et al., 2006; Ferreira, Pinto, Soares, & Soares, 2015). After pH adjustment, the samples were incubated at 40 °C under magnetic stirring (300 rpm) and aliquots (0.5 mL) were taken after 0, 1, 2, 4, and 24 h. During incubation, no measures were taken to reduce oxygen levels. The 0.5 mL samples were centrifuged (5 min, 15,000 × *g*) and the supernatant was separated to obtain the water soluble (WS) fraction. The pellet was solubilised with DMSO (100 % [*v/v*]), which is known to be a suitable solvent for metal:ligand systems (El-Sherif, Shoukry, & Abd-Elgawad, 2013). The resulting suspension was centrifuged once more (5 min, 15,000 × *g*) and the supernatant was separated to obtain the DMSO soluble (DS) fraction. The DMSO insoluble pellet was freeze-dried to remove any remaining DMSO. Subsequently, 200 μL of 25 mM aqueous ascorbic acid was added to the freeze-dried pellet, which was then sonicated for 15 min, diluted 20 times with DMSO for a final DMSO concentration of 95 % (*v/v*), and sonicated for an additional 15 min. After sonication, the sample was centrifuged for 5 min (15,000 × *g*) and the supernatant was collected as the ascorbic acid soluble (AAS) fraction. The remaining pellet was not analysed further. The colour of the samples was recorded and assessed by spectrophotometric analysis and by taking pictures (Samsung-G960F, Seoul, South Korea) against a white background.

2.3. Monitoring complexation, oxidation, and discolouration by UV–Vis spectroscopy

The effect of $FeSO_4$ addition on complexation and oxidation reactions, and their effect on discolouration was monitored using UV–Vis spectroscopy according to a method adapted from (Bijlsma et al., 2020). In short, the UV–Vis spectra of the WS and DS fractions were obtained directly after sampling and centrifugation, 200 μL sample was transferred to a Corning® UV-transparent flat-bottom polystyrene 96 well-plate (Sigma Aldrich, St. Louis, MO, USA). Spectra were recorded in the range from 250 to 750 nm in a SpectraMax M2e (Molecular Devices, Sunnyvale, CA, USA), at room temperature. The lower relative polarity of DMSO in the DS fractions (0.44) in comparison to water in the WS fractions (1.00) can affect electronic transitions and absorbance spectra (Reichardt & Welton, 2011). In this study, a maximum bathochromic shift of the $\pi \rightarrow \pi^*$ and $\pi \rightarrow d_\pi$ bands of 30 nm was observed in presence of DMSO.

2.4. Flavonoid quantification and identification of reaction products by RP-UHPLC-PDA-ESI-IT-MS^n

DS, WS, and AAS fractions were immediately analysed by reversed-phase ultra-high performance liquid chromatography coupled to electrospray ionisation ion trap mass spectrometry (RP-UHPLC-PDA-ESI-IT-MS^n). Flavonoids and their oxidation products were separated on a Thermo Vanquish UHPLC system (Thermo Scientific, San Jose, CA, USA) equipped with an autosampler, a pump, a photodiode array (PDA) detector, and coupled *in-line* to an LTQ Velos Pro ion trap mass spectrometer (Thermo Scientific). The temperature of the autosampler was controlled at 25 °C to prevent solidification of DMSO (T_m = 18.5 °C). Sample (1 μL) was injected on an Acquity UPLC BEH C18 column (150 mm × 2.1 mm i.d., 1.7 μm) with a VanGuard (5 mm × 2.1 mm i.d., 1.7 μm) guard column of the same material (Waters, Milford, MA). Water (A) and acetonitrile (B), both acidified with 0.1 % (*v/v*) formic acid, were used as eluents. The flow rate was 400 μL min^{-1}, and the temperature of the column oven was 45 °C with the post-column cooler set to 40 °C. The following elution profile was used: 0.00–1.09 min, isocratic on 1 % (*v/v*) B; 1.09–20.72 min, linear gradient from 1 to 55 % (*v/v*) B; 20.72–21.81 min linear gradient from 55 to 100 % (*v/v*) B; 21.81–27.26 min isocratic on 100 % (*v/v*) B; 27.26–28.35 min linear gradient from 100 to 1 % (*v/v*) B; 28.35–33.81 min isocratic on 1 % (*v/v*) B. The PDA detector was set to measure the wavelength range of 190–680 nm. Mass spectrometric data were acquired using an ion trap mass spectrometer equipped with a heated electrospray ionisation probe (ESI-IT-MS^n). Nitrogen was used as a sheath gas (50 arbitrary units) and auxiliary gas (13 arbitrary units). Data were collected over the *m/z* range of 100–1,500 in negative and positive ionisation mode by using source voltages of 2.5 and 3.5 kV, respectively. For both modes, the S-lens RF level was set at 67 %, the ion transfer tube temperature was 263 °C and the source heater temperature 425 °C. Data-dependent MS^2 analysis was performed on the most intense ion by collision-induced dissociation (CID) with normalised collision energy of 35 %. A dynamic mass exclusion approach was used, in which the most intense ion was fragmented 3 times and was subsequently excluded from fragmentation for the following 5 s, allowing data-dependent MS^2 of less intense co-eluting compounds. Data acquisition and processing were performed using Xcalibur (version 4.1, Thermo Scientific). Quantification of each flavonoid in the WS, DS, and AAS fraction was performed based on PDA peak area (280 nm) and an external calibration curve of the corresponding authentic standard (0.03–1 mM, in duplicate, $R^2 \geq 0.99$). The quantity of flavonoid over time was defined as recovery, in which the starting concentration of flavonoid (1 mM) was set as 100 % recovery. To test if the trend in flavonoid decrease over time was statistically significant, ANOVA analysis was performed using IBM SPSS Statistic v23 software (SPSS Inc., Chicago, IL, USA). Tukey's *post hoc* comparisons (significant at $p < 0.05$) were carried out to evaluate differences per time point in the total flavonoid recovery and recovery of flavonoid in the WS, DS, and AAS fraction.

2.5. Determination of iron concentration by ferrozine-based colourimetric assay

The total amount of iron in the WS, DS, and AAS fractions obtained at the different time points was quantified using a ferrozine-based colourimetric assay (Stookey, 1970). Binding of ferrous iron by 3-(2-pyridyl)-5–6-(bis(4-phenylsulfonic acid)-1,2,4-triazine (*i.e.* ferrozine) results in the formation of a complex with λ_{max} at 565 nm. To ensure the reduction of ferric iron to its ferrous state, an excess of ascorbic acid (50 μL, 100 mM) was added to 50 μL sample (*i.e.* WS, DS, AAS fractions). After 1 h incubation with ascorbic acid, an excess of ferrozine (50 μL, 10

mM) was added. Ferrozine is a highly ferrous-stabilising ligand, therefore all ferrous iron binds to ferrozine to yield a ferrous iron-ferrozine complex (Berker, Güçlü, Demirata, & Apak, 2010). Samples were transferred to 96-well microplates and the absorbance at 565 nm was measured in a SpectraMax M2e, at room temperature. All measurements were performed in duplicate, quantification of total iron was performed based on intensity (565 nm) and a calibration curve of $FeSO_4$ (0.00625–0.5 mM, in duplicate, $R^2 \geq 0.99$). Measurements were corrected for the flavonoid blank and it was confirmed that presence of DMSO did not interfere with the quantification of soluble iron.

2.6. Characterisation of the nature and morphology of iron-flavonoid reaction products

The nature and morphological characteristics of naringenin and quercetin samples prior to and after reaction with $FeSO_4$ but before fractionation to WS, DS, and AAS were analysed using X-ray powder diffraction (XRD), scanning electron microscopy (SEM), and transmission electron microscopy (TEM). The iron-flavonoid samples were prepared as described in section 2.2 and a sample was taken before ($t_{0'}$) and after adjustment of pH to 6.5 (t_0). XRD measurements were performed with a Bruker D8 Advance diffractometer (Bruker, Karlsruhe, Germany). The source consisted of Cu Kα radiation (λ = 1.54 Å). XRD patterns were recorded from 5° to 60° 2θ, with a step size of 0.01° and a scan speed of 0.1 s/step. The XRD data was processed using the Bruker DIFFRAC.EVA software and the obtained patterns were identified by comparison with reference patterns in the Crystallography Open Database (COD). Optical analysis was carried out at the Wageningen Electron Microscopy Centre (WEMC). Prior to SEM, iron-flavonoid sample was applied to a 1 μm filter and air-dried. The sample was attached on a sample holder using carbon adhesive tabs and sputter-coated with 12 nm tungsten using a Leica SCD 500 (Vienna, Austria). SEM analysis was performed on FEI Magellan 400 (FEI, Eindhoven, The Netherlands). For TEM analysis, 1 mM samples were added to a 400 mesh formvar/carbon grid and air-dried prior to measurement using a JEM-1400Plus (JEOL, MA, USA), operating at 120 kV.

3. Results and discussion

3.1. Effect of flavonoid structure on iron-mediated discolouration

Absorbance spectra of the flavonoid samples were recorded in the absence and presence of iron. Fig. 2A shows the λ_{max} values and colour of the flavonoid and flavonoid + iron samples at pH 6.5. Full absorbance spectra of the water soluble (WS) and DMSO soluble (DS) fractions of all ten flavonoids are shown in the supplementary information (Fig. SI-1 to SI-4).

Two characteristic π → π* bands were observed in absorbance spectra of all flavonoids possessing a 4-keto group in conjugation with the *C*2–*C*3 double bond, namely the benzoyl (A-ring) and cinnamoyl (B-ring) bands

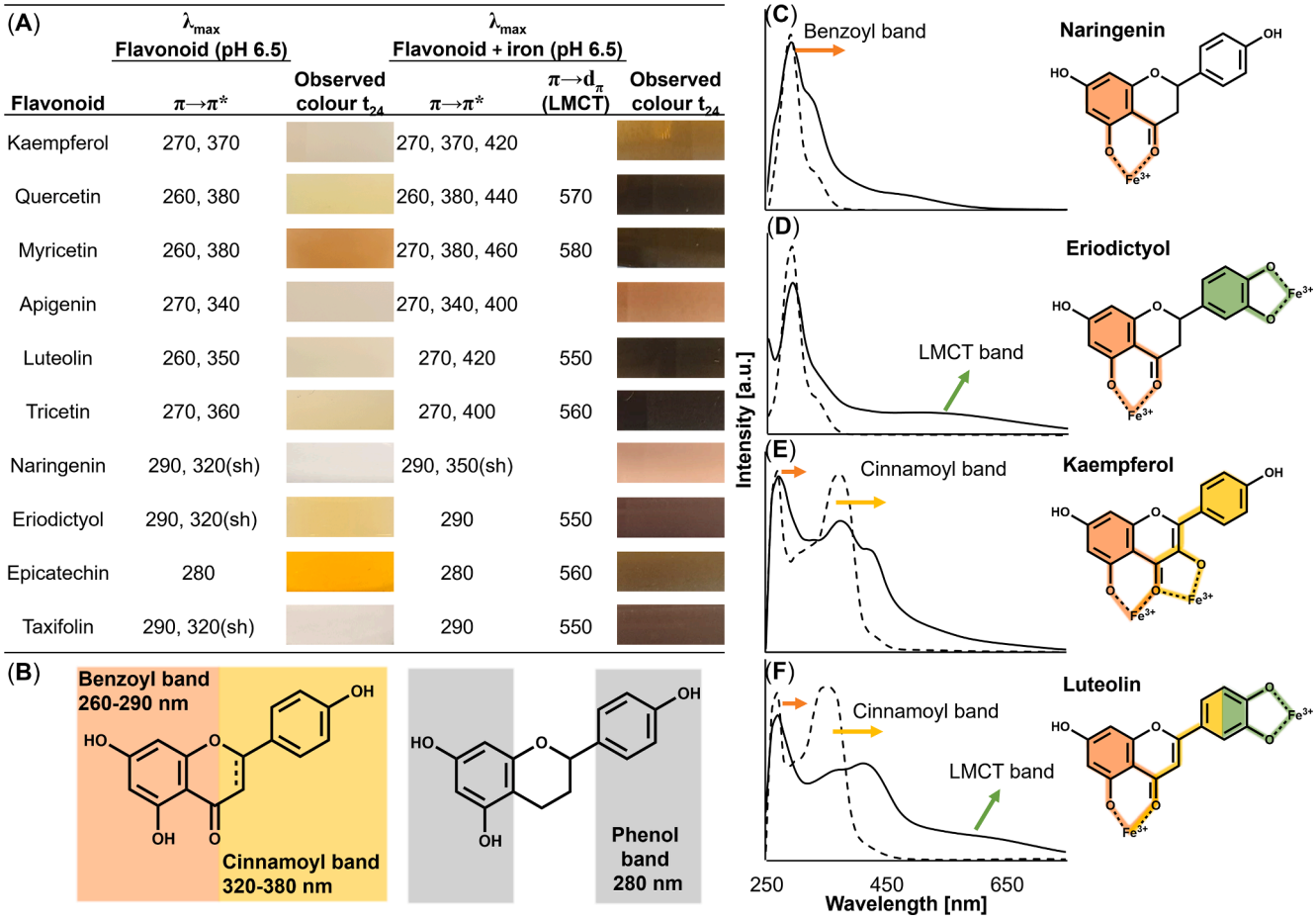

Fig. 2. (A) Maximum absorbance wavelength (λ_{max}) of the flavonoids in presence and absence of $FeSO_4$ at pH 6.5, and pictures of the observed colour in the sample after 24 h incubation; (B) structural moieties of flavonoids responsible for the main π → π* absorbance bands: the benzoyl band (orange), cinnamoyl band (yellow), and phenol band (grey). Combined WS and DS absorbance spectra of (C) naringenin; (D) eriodictyol; (E) kaempferol; and (F) luteolin in presence of $FeSO_4$ before pH adjustment ($t_{0'}$; dotted line) and after adjusting pH to 6.5 (t_0; solid line), the conjugated system responsible for LMCT is marked in green; the conjugated system responsible for the benzoyl band is marked in orange; the conjugated system responsible for the cinnamoyl band in yellow. (For interpretation of the references to colour in this figure legend, the reader is referred to the web version of this article.)

with λ_{max} values ranging from 260 to 290 nm and 320–380 nm, respectively (Fig. 2B). The absence of the *C*2–*C*3 double bond in the flavanones (*i.e.* naringenin, eriodictyol, and taxifolin) resulted in weak absorbance of the cinnamoyl band as a shoulder (sh) band (Dobashi, Hirano, Hirano, & Ohkatsu, 2008). Additionally, the larger conjugated system of flavonols and flavones led to a λ_{max} of the cinnamoyl band at higher wavelengths. Epicatechin lacks the 4-keto and *C*2–*C*3 double bond and therefore only showed a phenol band at 280 nm. Before adjustment of the pH to 6.5 ($t_{0'}$), no changes in the absorbance spectra of flavonoids were observed in the presence of $FeSO_4$ compared to the spectra of flavonoids in absence of $FeSO_4$. Generally, the iron-flavonoid samples at $t_{0'}$ were transparent or yellow and showed the same benzoyl, cinnamoyl, and phenol bands compared to the flavonoid blanks (supplementary information, Fig. SI-3 and SI-4). Upon adjusting the pH to 6.5, a bathochromic shift to wavelengths in the visible spectrum was observed (Fig. 2C-E). These findings indicate that deprotonation of the hydroxyl substituents is a prerequisite for complexation, which subsequently leads to fast discolouration. Normally, the pK_a value of the most acidic phenol moiety of flavonoids is around 9 but, because iron stabilises the deprotonated state, the apparent pK_a is in the range of 5–8 in the presence of iron (Hider, Liu, & Khodr, 2001; Perron & Brumaghim, 2009).

The structural features of flavonoids affected the electronic transition and the observed colour in presence of iron. The benzoyl $\pi \rightarrow \pi^*$ transition band broadened to higher wavelengths for naringenin (Fig. 2C). This flavanone contains only the 4–5 binding site and does not possess a *C*2–*C*3 double bond. Peak broadening resulted in an increased absorbance from 350 to 550 nm, which led to a light red-brown colour of these samples. Mellican et al. (2003) incubated similar concentrations of naringenin with ferric sulphate in pure water at pH 7. However, they reported that no colour formation was observed, even though their absorbance spectra also indicate an increase in absorbance from 400 to 650 nm, albeit at relatively low intensities.

Formation of a broad absorbance band (Fig. 2D) with a λ_{max} ranging from 550 to 560 was observed for flavonoids possessing the 3'-4' binding site (*i.e.* catecholate) but lacking the *C*2–*C*3 double bond (*i.e.* eriodictyol, epicatechin, and taxifolin). This wavelength is typical for LMCT in Fe^{3+}-catecholate complexes at pH ranging from 5 to 7 and caused the purplish appearance of these samples (Bijlsma et al., 2020; Elhabiri et al., 2007). Besides their 3'-4' binding site, eriodictyol and taxifolin also possess the 3–4 and 4–5 iron-binding sites. However, the absence of the *C*2–*C*3 double bond does not allow electron delocalization through the whole structure, as a result, absorbance spectra of these flavonoids were dominated by the LMCT band (Fig. 2D, supplementary information, Fig. SI-4E&I).

Bathochromic shifting of the benzoyl and cinnamoyl $\pi \rightarrow \pi^*$ band was observed for kaempferol and apigenin, both of which contain the 4–5 binding site in conjugation with the *C*2–*C*3 double bond (Fig. 2E). This bathochromic shifting was previously assigned to an extension of the conjugated π-π system induced by the positively charged metal (Guo et al., 2007). Discolouration of these samples resulted from the extended conjugated system, leading to increased absorbance in the visible spectrum. The bathochromic shift of the cinnamoyl band of kaempferol was more intense than that of apigenin and shifted to higher wavelengths, as kaempferol possesses the 3–4 binding site in addition to the 4–5 binding site.

Bathochromic shifting of the benzoyl band and cinnamoyl band was also observed for flavonoids containing the 3'-4' binding site, and the 4–5 binding site in conjugation with the *C*2–*C*3 double bond (*i.e.* quercetin, myricetin, luteolin, tricetin) (Fig. 2F). Additionally, for these flavonoids a broad absorbance band was observed at higher wavelengths, resulting from $\pi \rightarrow d_\pi$ transitions (*i.e.* LMCT) of the catechol or pyrogallol moiety and the complexed iron. The combination of the bathochromic shift of the cinnamoyl band ($\pi \rightarrow \pi^*$) band and LMCT band ($\pi \rightarrow d_\pi$) resulted in intense discolouration (Fig. 2A).

To summarise, discolouration was observed for all tested flavonoids in presence of iron at pH 6.5. Moreover, the electronic transition responsible for discolouration was defined by the structural features of the flavonoid. The presence of the combination of the catechol moiety, the 4-keto, and the *C*2–*C*3 double bond resulted in the most intense colour by a combination of bathochromic shifting of the cinnamoyl band ($\pi \rightarrow \pi^*$) and LMCT phenomena ($\pi \rightarrow d_\pi$). Presence of the 3-hydroxy group provided an additional binding site and therefore resulted in more intense discolouration.

3.2. Solubility and stability of flavonoids in presence of iron

The recovery of flavonoid over time in presence of iron was quantified by RP-UHPLC-PDA-MS^n (Fig. 3). An overview of the mass spectrometric and spectroscopic data used to identify the flavonoids is provided in the supplementary information (Table SI-1). Total recovery of flavonoid was followed over time in three different fractions, water soluble (WS), DMSO soluble (DS), and ascorbic acid soluble (AAS). Iron-flavonoid complexes were unstable in the LC mobile phase (*i.e.* water/acetonitrile with 0.1 % formic acid) because of protonation of the flavonoid at the acidic conditions (Krabbe, Lingeman, Niessen, & Irth, 2005). Therefore, only free flavonoids were identified and quantified, which could directly be linked to the solubility and extent of oxidation. Before adjustment of the pH ($t_{0'}$), high recoveries were found for all flavonoids. Flavonoids with the *C*2–*C*3 double bond showed poor water solubility, as evidenced by their recovery in DS compared to WS, due to their planar ring structure facilitating hydrophobic interaction by π-π stacking of the aromatic nuclei in aqueous environments.

For the flavonoids with a pyrogallol moiety on the B-ring, *i.e.* myricetin and tricetin, a decreased recovery was observed over time, with respective losses of 78 % and 70 % of the initial amount after 24 h incubation. Pyrogallol moieties generally have a lower pK_a than catechol moieties, resulting in a higher phenoxide concentration at pH 6.5, making the flavonoid more prone to oxidation (Habeych et al., 2016; Jovanovic, Simic, Steenken, & Hara, 1998). For quercetin also a significant decrease of 14 % was observed after 24 h incubation. The iron-mediated oxidation rate increased due to the presence of the 3-hydroxy group (quercetin vs. luteolin) as well as the *C*2–*C*3 double bond (quercetin vs. taxifolin). For epicatechin, which lacks the 4-keto moiety, a loss of 87 % was observed over time. It is well-established that epicatechin can easily be oxidised to brown-coloured coupling products by enzymatic oxidation and auto-oxidation (Tan et al., 2020). The absence of the 4-keto group on epicatechin likely results in reduced oxidative stability compared to the other flavonoids tested.

For kaempferol, taxifolin, apigenin, luteolin, naringenin, and eriodictyol, no significant decrease was observed over 24 h of incubation in presence of iron ($p > 0.05$). For some flavonoids, in particular those that possess multiple iron-binding sites, adjustment to pH 6.5 led to the formation of black precipitate that was only soluble after the addition of an excess of ascorbic acid (AAS). In section 3.4 this phenomenon will be further discussed.

As a control, all flavonoids were also incubated at pH 6.5 over time in absence of iron (supplementary information, Fig. SI-5). Most flavonoids were stable over 24 h aqueous incubation in absence of iron. However, myricetin and epicatechin showed decreases of 45 % and 22 % in total recovery after 24 h incubation, respectively. Auto-oxidation of flavonoids in an aqueous solution occurs via electron transfer (ET) reactions. Myricetin possesses all structural features essential for oxidation (*i.e.* 3-OH, 4'-OH, and *C*2–*C*3 double bond) and is therefore also prone to auto-oxidation. However, the 78 % decrease in myricetin recovery in presence of iron shows that the oxidation reaction is accelerated by iron. In presence of iron, the degradation of tricetin was similar to myricetin (70 % vs. 78 % in 24 h). In absence of iron, no significant decrease was observed for tricetin. Tricetin lacks the 3-OH group, and cannot form quinone methides, which are chemically more reactive and unstable than *ortho*-quinones (Stepanic, Gasparovic, Troselj, Amic, & Zarkovic, 2015).

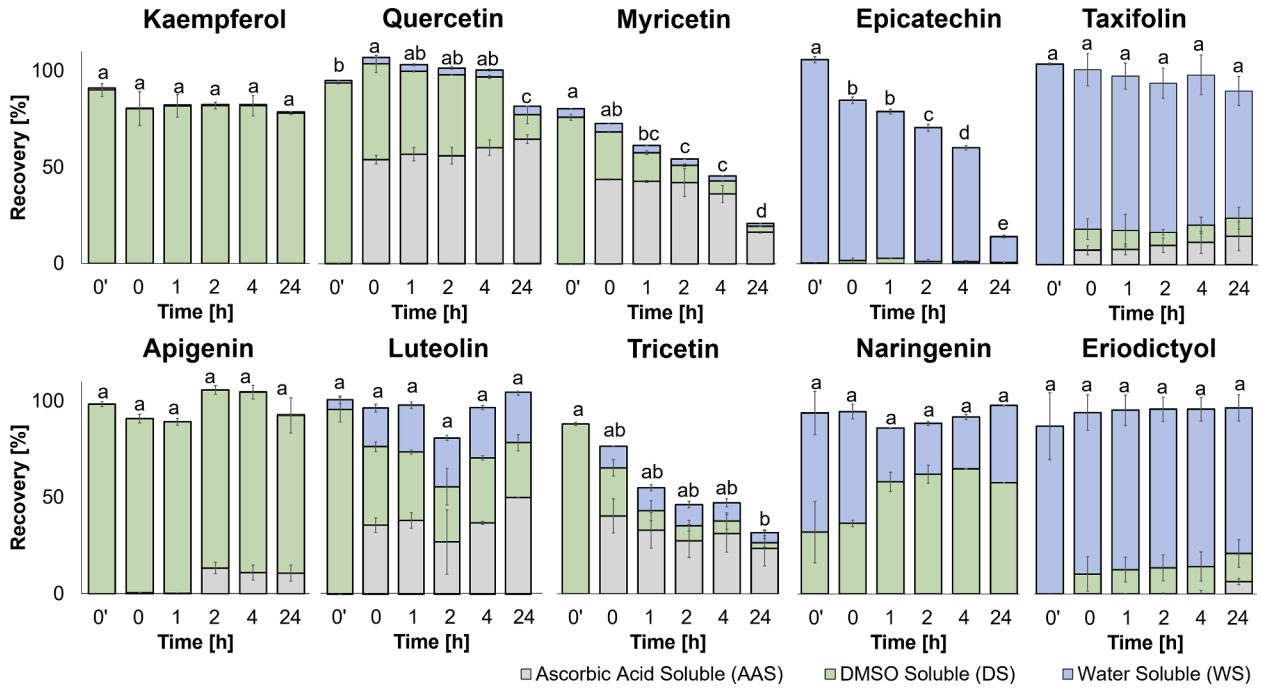

Fig. 3. Recovery of kaempferol, quercetin, myricetin, epicatechin, taxifolin, apigenin, luteolin, tricetin, naringenin, and eriodictyol in the WS (blue), DS (green), and AAS (grey) fractions in presence of iron before adjustment of the pH ($t_{0'}$) and after 0, 1, 2, 4, and 24 h of incubation at pH 6.5. Error bars indicate the standard deviation of independent duplicates. Different letters indicate a significant difference in total recovery compared to other time points for the same flavonoid (Tukey's test, $p < 0.05$). Significance of differences in the three individual fractions (*i.e.* WS, DS, and AAS) per time point for each flavonoid is indicated in the supplementary information, Table SI-3. (For interpretation of the references to colour in this figure legend, the reader is referred to the web version of this article.)

3.3. Flavonoid oxidation in the presence of iron

The complexation reaction can be followed up by ET reactions that cause oxidation of flavonoids, as evidenced by the decreased recovery of flavonoids over time (Fig. 3). These ET reactions yield a plethora of oxidation products by degradation or oxidative coupling reactions. The formation of flavonoid oxidation products was monitored by RP-UHPLC-PDA-MS^n. The major oxidation products present in the WS and DS fractions were tentatively identified based on spectrometric and spectroscopic data (Table SI-2). The RP-UHPLC-PDA chromatograms of quercetin with $FeSO_4$ before and after 24 h of incubation (Fig. 4A) show that aqueous incubation of quercetin with $FeSO_4$ resulted in the formation of several oxidation products. Chromatograms of the other flavonoids before pH adjustment ($t_{0'}$) and after 24 h incubation at pH 6.5 are provided in the supplementary information (Fig. SI-6 and SI-7). An overview was created of the main characteristic degradation end products and coupling products formed per flavonoid after 24 h of incubation (Fig. 4B). The oxidation products could not be quantified because the molar extinction coefficients of some of the formed compounds were unknown. However, the cumulative PDA (250 to 400 nm) peak areas of the chromatograms were used as an indication for the total amount of oxidation products formed (Fig. 4C), as all oxidation products showed λ_{max} values within this range.

3.3.1. Degradation reactions

The main characteristic degradation products formed by iron-mediated oxidation of flavonoids in aqueous solution were 4-hydroxybenzoic acid (4-HBA), 3,4-dihydroxybenzoic acid (3,4-DHBA; protocatechuic acid), or 3,4,5-trihydroxybenzoic acid (3,4,5-THBA; gallic acid), 2,4,6-THBA (*i.e.* phloroglucinol carboxylic acid), and 2,4,6-trihydroxyphenylglyoxilic acid (2,4,6-THPGA). The proposed pathway of Fe^{3+}-mediated oxidative degradation of quercetin is illustrated in Fig. 4D. After complexation of quercetin to Fe^{3+} (**1**), ET from quercetin to Fe^{3+} leads to formation of a semiquinone (not shown) and upon a second ET an *ortho*-quinone (**2**) is formed. This *ortho*-quinone readily isomerises to a *para*-quinone methide intermediate (**3**), which is converted to a flavylium cation upon protonation (**4**, **5**). Subsequent hydroxylation at the *C*2 position leads to formation of an unstable 2,5,7,3'-4'-pentahydroxy-3,4-flavandione (**6**). Via ring-opening the intermediate 5,7,9,3'-4'-pentahydroxy-2,3,4-chalcantrione (**7**) is formed, this molecule is also unstable, and may rearrange to form the intermediate 2-(3'-4'-dihydroxybenzoyl)-2,4,6-trihydroxybenzofuran-3(2H)-one (**8**) (Sokolová et al., 2016). Moreover, product **7** can undergo hydrolysis resulting in formation of lower molecular weight products. Cleavage of the *C*2–*C*3 bond results in formation of the A-ring derived 2,4,6-THPGA (***P*1**) and B-ring derived 3,4-DHBA (***P*2**). Moreover, cleavage of the *C*3-*C*4 bond results in the formation of A-ring derived 2,4,6-THBA (***P*3**) and B-ring derived 3,4-DHPGA (***P*4**) (Fig. 4D). For all investigated flavonoids, except epicatechin, a distinct peak was observed in UHPLC-PDA-MS^n with a difference in *m/z* of 16 amu, probably this corresponds to one of the hydroxylated intermediates. Based on the mass spectrometric data and the fragmentation profile, which show RDA fragmentation typical for (oxidised) flavonoids. It seems unlikely that this peak was chalcantrione (**7**), as we would expect to observe a distinct MS^2 fragmentation profile resulting from cleavage between the more labile *C*2 and *C*3 or *C*3 and *C*4 positions in the MS. Therefore, it is expected that this peak corresponds to either the flavandione (**6**) or benzofuranone (**8**) (supplementary information, Table SI-2). We cannot presently distinguish between these two intermediate oxidation products (Zhou & Sadik, 2008).

If the 3-OH group was present in conjugation with the *C*2–*C*3 double bond (flavonols), degradation to hydroxybenzoic acid derivatives was more prominent compared to the other flavonoid subclasses. The presence of these functional moieties enabled the formation of the highly reactive quinone methides. As a result, oxidative degradation was preferred over oxidative coupling for flavonols, which is in line with previous findings regarding flavonol oxidation in aqueous environments (Pinelo, Manzocco, José Nuñez, & Cristina Nicoli, 2004). In absence of the 3-OH group (*i.e.* flavones) only *ortho*-quinones can be formed, which are relatively more stable in aqueous solution than quinone methides, resulting in slower oxidation (Stepanic et al., 2015). Similarly, in

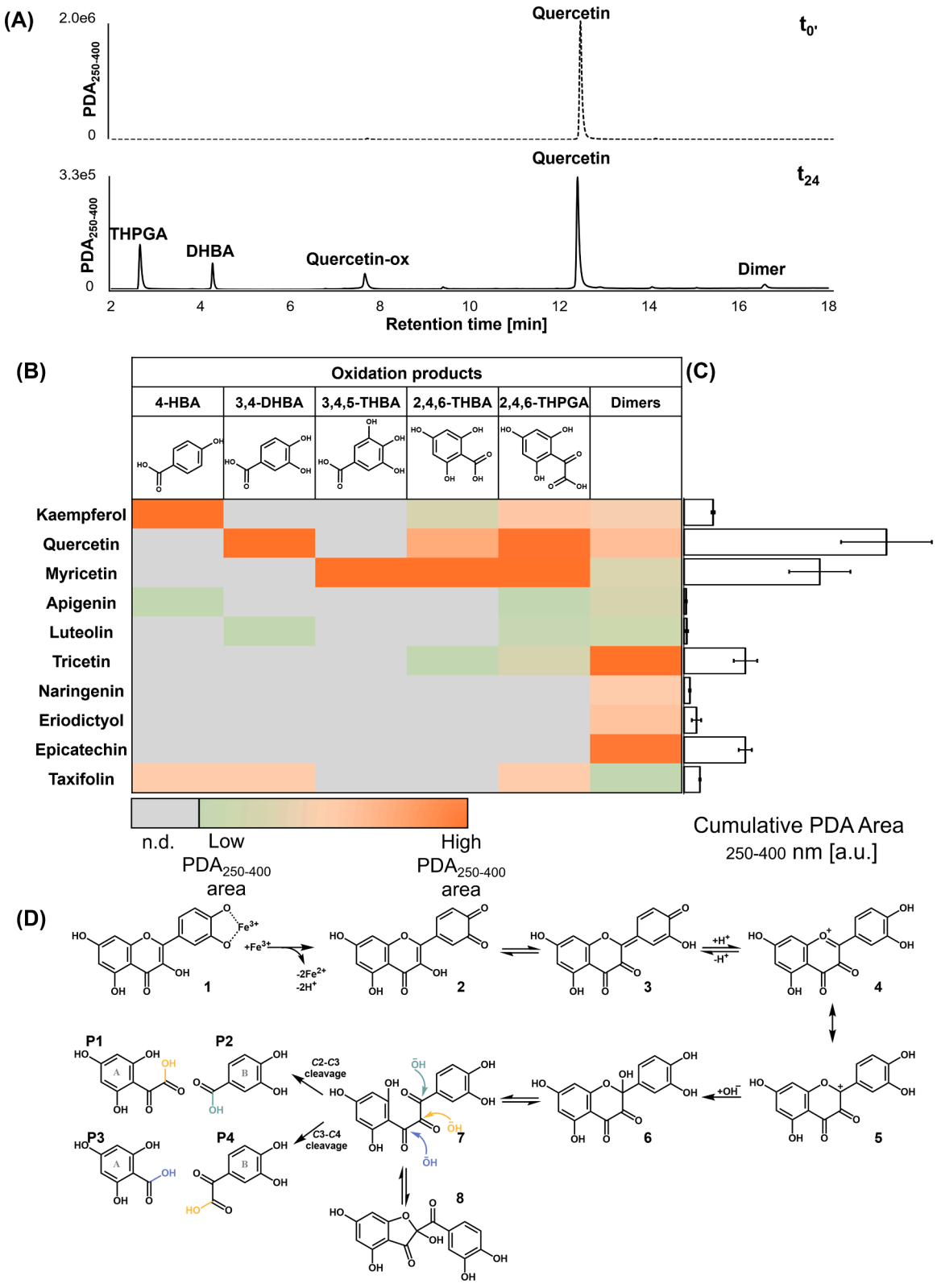

Fig. 4. (A) RP-UHPLC-PDA (250–400 nm) profiles of quercetin × $FeSO_4$ samples before incubation and pH adjustment ($t_{0'}$) and after 24 h incubation pH 6.5, 40 °C (t_{24}). (B) Heatmap indicating the type and relative quantity of individual oxidation products formed per flavonoid after incubation for 24 h. Tentative identification of these compounds is based on Table SI-2 (supplementary information), colour indicates the relative levels per oxidation product (grey = n.d., not detected; green = low $PDA_{250\text{-}400}$ area; and orange = high $PDA_{250\text{-}400}$ area). (C) Cumulative area of PDA peaks for oxidation products after 24 h of incubation, detected in the wavelength range of 250–400 nm. (D) Proposed pathway of Fe^{3+}-mediated oxidative cleavage of flavonols on the *C*2–*C*3 or *C*4-*C*5 position (illustrated for quercetin). HBA = hydroxybenzoic acid, DHBA = dihydroxybenzoic acid, THBA = trihydroxybenzoic acid, THPGA = trihydroxyphenylglyoxylic acid. (For interpretation of the references to colour in this figure legend, the reader is referred to the web version of this article.)

absence of the *C*2–*C*3 double bond (*i.e.* taxifolin) also limited formation of degradation products was observed. If both of these moieties were absent (*i.e.* naringenin, eriodictyol, and epicatechin), no degradation products were observed.

Formation of degradation products over time lowered the absorbance in the visible range, as shown in the absorbance spectra of quercetin and myricetin (supplementary information, Fig. SI-3). A decrease was observed in the absorbances of both the LMCT band and the cinnamoyl-iron bands. Simultaneously, a new peak with λ_{max} at 290 nm appeared, resulting from the formed hydroxybenzoic acid derivatives that possess one phenolic moiety and a limited conjugated system. This decrease in absorbance in the visible range due to oxidation is in line with previous research on fading of the colour of aluminium-flavonoid complexes due to metal-mediated oxidation (Smith, Thomsen, Markham, Andary, & Cardon, 2000). Preliminary experiments (results not shown) indicated that incubation of quercetin with iron under the same conditions for an extended time (*i.e.* weeks) prompted the formation of a new LMCT band, most likely resulting from complexation of the hydroxybenzoic acid derivatives to iron.

3.3.2. Oxidative coupling reactions

Oxidative coupling of the flavonoids in presence of Fe^{3+} was also followed by RP-UHPLC-PDA-MS. Dimers were detected by creating extracted ion chromatograms with a dimer mass range of $((M_w \times 2) - 2) \pm 5$, and were tentatively identified based on their mass spectra. Detailed mass spectrometric and spectroscopic data of the dimers is provided in the supplementary information (Table SI-2). All identified dimers were dehydro-type dimers. Extracted ion chromatograms for specific *m/z* values that correspond to benzotropolone-type dimers (*e.g.* theaflavins) indicated that none of these types of dimers was formed. These findings are in line with recent work on the auto-oxidative browning mechanism of epicatechin, in which it was shown that dehydrodicatechins were the main products of epicatechin auto-oxidation (Tan et al., 2020). Thus, the iron-mediated dimerisation pathway is hypothesised to follow a similar mechanism as auto-oxidative dimerisation. Dimer formation was more prominent in the flavonoids lacking the *C*2–*C*3 double bond. Additionally, dimerisation was also observed for tricetin, which does possess the *C*2–*C*3 double bond. Thus, we suggest that the absence of the 3-OH group stabilised tricetin against undergoing degradation reactions, thereby directing the reaction towards oxidative coupling, resulting in dimer formation. Extracted ion chromatograms were also screened for trimers and oligomers. Except for epicatechin trimers, no tri- or oligomers were detected.

Flavonoid oxidative coupling is hypothesised to contribute to discolouration in two ways: (i) the dimers' extended conjugated systems give a brownish colour; and (ii) the dimers can form coloured complexes with iron. Most of the flavonoid dimers that were identified by UHPLC-PDA-MS had a λ_{max} ranging from 350 to 400 nm and thus showed absorbance in the visible light range (380–750 nm). However, even after 24 h, the relatively small amount of dimers formed via oxidative coupling did not affect the full absorbance spectra of the iron-flavonoid samples, except for epicatechin. The UV–Vis absorbance spectra of epicatechin in presence of iron (supplementary information, Fig. SI-8) indicated increased absorbance between 400 and 500 nm, resulting from the formation of brown coloured epicatechin dimers and trimers. In addition to this broad absorbance "hump", the LMCT band with a λ_{max} around 550 nm was also still present, indicating the presence of iron-flavonoid complexes. Interaction of the epicatechin with iron resulted in a purplish colour, whereas interaction of the dimers and trimers with iron resulted in black colour formation due to the extended conjugated system and a combination of $\pi \rightarrow \pi^*$ and $\pi \rightarrow d_\pi$ transitions (supplementary information, Fig. SI-8). Furthermore, the number of iron-binding sites increases with the degree of polymerisation, as additional binding sites arise from hydroxyl/carbonyl groups.

Overall, iron-mediated oxidation reactions of flavonoids led to degradation or oxidative coupling, that resulted in a decrease or increase in visible light absorbance, respectively. Considering the trends observed here, it is expected that upon incubation for more than 24 h, these colour changes will become more pronounced.

3.4. Formation of iron-flavonoid networks

The samples of quercetin, myricetin, luteolin, and tricetin with $FeSO_4$ showed the formation of black particles with poor solubility and the flavonoids were only recovered after the addition of an excess of ascorbic acid (AAS) (Fig. 3). Recovery of flavonoids in the AAS fraction indicated that the poor solubility of flavonoids in presence of iron was caused by a reversible interaction (*i.e.* complexation). Disruption of the reversible iron-flavonoid interactions by addition of ascorbic acid can be due to protonation of the hydroxyl groups at low pH, reduction of Fe^{3+} to Fe^{2+}, competition by ascorbic acid for iron complexation, or a combination thereof. Exploratory experiments with concentrated HCl indicated that solely lowering the pH was sufficient to disrupt the iron-flavonoid interactions (results not shown). The main flavonoids that showed precipitation in our study (*i.e.* quercetin, myricetin, luteolin, and tricetin) possessed the 3–4 site and/or the 4–5 site in combination with the 3'-4' site. We, therefore, concluded that multiple iron-binding sites on flavonoids were a prerequisite for the formation of poorly soluble interaction products. Habeych et al. (2016) also observed precipitate formation of phenolic compounds with multiple binding sites in presence of $FeSO_4$. These authors interpreted precipitation as either oxidation of phenolics to polymers, or formation of high molecular size networks by bridging of phenolics with iron, though neither of these mechanisms were confirmed (Habeych et al., 2016). Based on the reversibility of our iron-flavonoid interactions by the addition of ascorbic acid, we hypothesise that precipitation was mainly the result of the formation of insoluble complexes or networks rather than covalent oxidative coupling. In another study, it was also reported that myricetin, quercetin, and luteolin can form Fe^{3+}-coordinated metal-phenolic networks (MPN) (Bertleff-Zieschang et al., 2017). MPNs are supramolecular networks of metal ions coordinated to phenolic ligands and are commonly characterised by an amorphous nature (Ejima, Richardson, & Caruso, 2017; Rahim et al., 2015). To confirm that MPNs were formed, the nature and morphology of the iron-flavonoid interaction products were analysed by powder X-ray diffraction (XRD). For these experiments, we selected two samples: iron-quercetin, representing flavonoids with two binding sites, and iron-naringenin, representing flavonoids with one binding site (Fig. 5).

The XRD patterns of quercetin (Fig. 5A) and naringenin (Fig. 5D) showed crystalline patterns that were respectively identified as triclinic quercetin dihydrate and monoclinic naringenin. XRD patterns of mixed iron-flavonoid samples at $t_{0'}$ showed crystalline peaks indicative for a mixture of the flavonoid and $FeSO_4$ without any interaction (Fig. 5B, 5E). The XRD pattern of the iron-flavonoid samples after pH adjustment to 6.5 (Fig. 5C, 5F) showed a broad "hump" caused by diffuse scattering. This broad "hump" is indicative for the disordered nature of an amorphous material. This is in line with previously reported results on the amorphous nature of the reaction product of iron with quercetin at pH 12 (Papan, Kantapan, Sangthong, Meepowpan, & Dechsupa, 2020). The XRD patterns of the iron-flavonoid samples after pH adjustment to 6.5 (Fig. 5C, 5F) were distinctly different from those obtained for $FeSO_4$ on its own after pH adjustment to 6.5 (supplementary information, Fig. SI-9). Thus, we confirmed that the observed amorphousness is caused by an interaction between iron and the flavonoid and not by the formation of iron (oxy)hydroxide species. Also naringenin, for which no AAS fraction was observed, yielded an XRD pattern corresponding to an amorphous material. The amorphousness of iron-flavonoid reaction products can be a result of the formation of MPNs. Wang (2013) also showed that amorphousness may indicate the formation of iron-phenolic complex nanoparticles with a 1:3 stoichiometry (Rahim et al., 2015; Wang, 2013). The existence of coordination-driven bridging interactions between iron and flavonoids via μ-oxo/hydroxo-

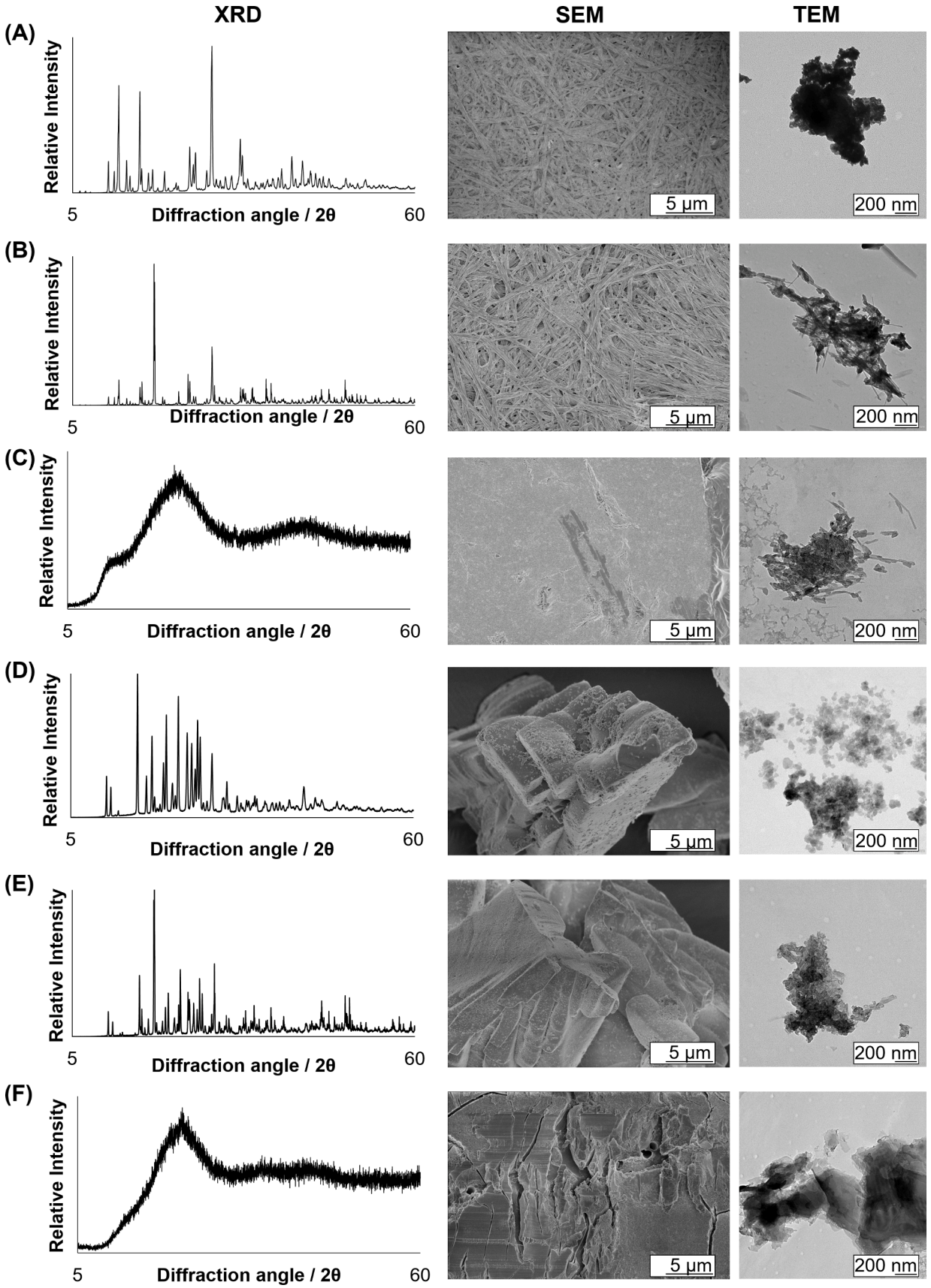

Fig. 5. Powder XRD patterns, SEM images, and TEM images for (A) quercetin; (B) quercetin × $FeSO_4$ (before pH adjustment, $t_{0'}$); (C) quercetin × $FeSO_4$ (pH = 6.5, t_0); (D) naringenin; (E) naringenin × $FeSO_4$ (before pH adjustment, $t_{0'}$); and (F) naringenin × $FeSO_4$ (pH = 6.5, t_0).

bridged Fe^{3+} species can also result in amorphous MPNs (supplementary information, Fig. SI-10) (Rahim et al., 2015; Zhong et al., 2019). Although the amorphous nature of the samples was a clear indication of the formation of more intricate iron-flavonoid interaction products, the XRD patterns on their own did not provide sufficient insight in these products' exact structural characteristics. To further investigate the potential presence of MPNs in our iron-flavonoid samples, electron microscopic measurements were performed.

SEM images of quercetin showed rod-like or needle-like shapes representing its high crystallinity (Fig. 5A). After the addition of $FeSO_4$ and adjustment of pH, the surface morphology became a dense, uniform, smooth film with an amorphous nature (Fig. 5C), further supporting the hypothesis that insoluble MPNs were present in the sample (Papan et al., 2020). For naringenin, the morphology also changed after the addition of $FeSO_4$ and pH adjustment (Fig. 5E). The surface morphologies of the iron-quercetin and iron-naringenin samples was distinctively different. The higher surface roughness and fracturing observed in the iron-naringenin sample compared to the iron-quercetin sample are indicative for discontinuous MPNs or nanoparticle deposition, rather than continuous extended MPNs.

TEM was performed on the iron-flavonoid samples in suspension. TEM images of pure quercetin show aggregation (Fig. 5A). High electron density led to intense Bragg reflections and dark contrast in the TEM image. Upon addition of $FeSO_4$ and before pH adjustment, the structure of quercetin still appeared needle-like and crystalline in SEM, but particles showed less aggregation in TEM (Fig. 5B). After adjustment to pH 6.5 characteristic needle-shaped structures were visible representing precipitated quercetin (Patel, Heussen, Hazekamp, Drost, & Velikov, 2012). In addition to that, irregularly shaped particles with morphologies in accordance with those of MPNs were revealed (Fig. 5C). This formation of networks was not observed for quercetin on its own. For naringenin, TEM revealed the presence of large aggregates, and the addition of $FeSO_4$ did not have much influence on their size or morphology (Fig. 5D, 5E). The addition of iron to naringenin and pH adjustment to 6.5 led to the formation of amorphous particles of increased size (Fig. 5F).

Based on these results obtained for quercetin and naringenin, we concluded that formation of MPNs occurred in both samples upon addition of iron and adjustment of pH to 6.5. The presence of a binding site on the 3–4 site and/or the 4–5 site in combination with the 3'-4' site, as in quercetin, was a prerequisite to form continuous extended MPNs. Moreover, the higher AAS recovery of the flavone and flavonol subclasses compared to the flavan subclasses (Fig. 3) indicated that the presence of the *C*2–*C*3 double bond enhanced the formation of insoluble extended MPNs. Based on the results obtained for naringenin, we propose that even flavonoids with only one iron-binding site can form MPNs. The number of interactions per flavonoid and molecular size of the resulting amorphous interaction products of these flavonoids with only one iron-binding site is expected to be much lower compared to MPNs from flavonoids with multiple iron-binding sites. Therefore, flavonoids with only one iron-binding site had higher solubility, as shown by the fact that they were mainly recovered in the WS and DS fractions, rather than the AAS fractions. We suggest that the large conjugated system of insoluble, extended MPNs is responsible for the strong black discolouration of the observed precipitate (*i.e.* AAS fraction). Furthermore, we speculate that the reduced solubility of these MPNs may also lead to decreased bio-accessibility compared to smaller, soluble complexes.

3.5. Implications of iron-flavonoid interactions on bio-accessibility of iron

In addition to flavonoid solubility, total iron solubility (as defined by Eq. (1)) was assessed.

$$[Fe]_{total} = [Fe]^{2+} + [Fe]^{3+} + \sum [Soluble\ products\ of\ Fe^{2+}\ and\ Fe^{3+}]$$

An overview of the recovery of iron, as determined by the ferrozine-based colourimetric assay, in the WS, DS, and AAS fractions are provided in the supplementary information (Fig. SI-11). The recovery of total iron in the water soluble (WS) fraction (Fig. 6) indicates its bio-accessibility (Wienk et al., 1999). The total iron solubility of the $FeSO_4$ control after pH adjustment to 6.5 decreased by 99 % due to the formation of poorly soluble iron (oxy)hydroxide species and hydrolytic polymers upon Fe^{3+} hydrolysis around neutral pH (Flynn, 1984; Wienk et al., 1999). The total solubility of iron in water at pH 6.5 was enhanced for most flavonoids in comparison to the control. The highest iron recovery was observed for the less planar flavonoids (*i.e.* flavonoids without the *C*2–*C*3 double bond), which also had a relatively high recovery of flavonoid in the WS fraction (Fig. 3). Moreover, it was observed that iron solubility was enhanced if two or more hydroxyl groups were present on the flavonoid B-ring. Complexation of Fe^{3+} to catechol stabilises Fe^{3+} against the formation of hydrolysis products (Bijlsma et al., 2020). On the other hand, combining iron with poorly water soluble flavonoids (*i.e.* kaempferol, quercetin, myricetin, apigenin, and naringenin) leads to precipitation of the complexes and/or MPNs, and thereby to low iron recovery in the WS fraction. The slight increase in iron solubility in the presence of some poorly water soluble flavonoids (*e.g.* quercetin and myricetin) over time indicates that their oxidative degradation products (*i.e.* hydroxybenzoic acid derivatives) may form water soluble complexes with iron.

Most iron absorption occurs in the duodenum (pH 6–6.5) and the upper jejunum (pH 7–9) (Wienk et al., 1999). Therefore, higher total recoveries of iron in the WS fraction in presence of flavonoids at pH 6.5 are indicative for better bio-accessibility, which is defined as the quantity of iron in solution and available for absorption in the gastrointestinal tract. It should be noted that although bio-accessibility of iron is a prerequisite for bioavailability, iron bio-accessibility cannot directly be correlated to iron bioavailability, which also includes digestion, absorption, and metabolism (Wienk et al., 1999). Nonetheless, based on these results, we expect that the formation of soluble iron-flavonoid complexes can still negatively affect iron bioavailability. Previous research on iron homeostasis in presence of quercetin and epigallocatechin gallate indicated an increase in apical uptake for the complexed iron, but a decrease in basolateral transport, leading to an overall reduction in iron bioavailability (Lesjak & Srai, 2019).

4. Conclusions

This is the first time that the combined effect of complexation, oxidation, and formation of networks on iron-mediated flavonoid discolouration, and the effect of flavonoids' structural features thereon, was investigated. Complexation of iron to all investigated flavonoids

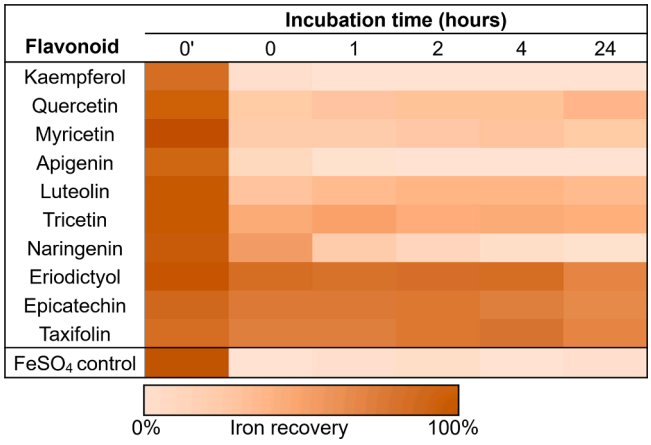

Fig. 6. Heatmap showing total iron solubility over time in the WS fraction for the $FeSO_4$ control and after incubation of $FeSO_4$ with different flavonoids.

resulted in fast discolouration in aqueous samples at pH 6.5. Binding of iron to the 3–4 site or 4–5 site resulted in bathochromic shifting of the cinnamoyl and/or benzoyl ($\pi \rightarrow \pi^*$) bands. In accordance with the hypothesis, the presence of the 3'-4' site (*i.e.* catechol or pyrogallol moiety) was a prerequisite for the formation of an LMCT ($\pi \rightarrow d_\pi$) band. Flavonoids possessing the 3'-4' site in conjugation with the *C*2–*C*3 double bond, and the 4–5 site showed the most intense discolouration, resulting from a combination of bathochromic shifting of the cinnamoyl band and LMCT phenomena. In addition to more intense discolouration, the presence of the *C*2–*C*3 double bond and more hydroxyl groups on the B-ring also led to a greater extent of iron-mediated oxidation reactions. The presence of the 3-hydroxy group also enhanced oxidative degradation by the formation of highly reactive quinone methides as reaction intermediates. Oxidative degradation or oxidative coupling of the flavonoid, respectively resulted in a decrease or increase in visible light absorbance. With XRD, SEM, and TEM, we confirmed that the black precipitate formed when iron was incubated with flavonoids that possess multiple iron-binding sites, was the result of the formation of extended MPNs. These extended MPNs likely possessed a higher number of interactions and molecular size compared to MPNs from flavonoids with only one iron-binding site. Additionally, the water solubility of iron in the presence of flavonoids was enhanced by flavonoids that possessed the 3'-4' binding site but lacked the *C*2–*C*3 double bond. This study shows that the structural features of flavonoids strongly influence their interactions with iron via complexation and oxidation, thereby affecting the resulting discolouration and formation of networks. In future work, it should be explored how these mechanistic insights in iron-flavonoid interactions can be used to develop approaches to prevent discolouration in novel mineral-fortified foods.

CRediT authorship contribution statement

Judith Bijlsma: Conceptualization, Methodology, Investigation, Data curation, Writing – original draft, Visualization. **Wouter J.C. de Bruijn:** Conceptualization, Methodology, Supervision, Writing - review & editing. **Krassimir P. Velikov:** Supervision, Writing - review & editing. **Jean-Paul Vincken:** Conceptualization, Supervision, Writing - review & editing.

Declaration of Competing Interest

The authors declare that they have no known competing financial interests or personal relationships that could have appeared to influence the work reported in this paper.

Acknowledgements

We would like to thank Marcel Giesbers and Jelmer Vroom from the Wageningen Electron Microscopy Centre (WEMC) for carrying out TEM and SEM data collection. Ilse Gerrits is kindly acknowledged for her help with the X-Ray powder diffraction measurements. The authors are thankful to Cas Geerits for his contribution to the preliminary data processing. This research received funding from the Netherlands Organisation for Scientific Research (NWO) in the framework of the Innovation Fund for Chemistry and from the Ministry of Economic Affairs in the framework of the "*TKI/PPS-Toeslagregeling*".

Appendix A. Supplementary data

Supplementary data to this article can be found online at https://doi.org/10.1016/j.foodchem.2021.131292.

References

Allen, L. H., De Benoist, B., Dary, O., & Hurrell, R. (2006). Guidelines on food fortification with micronutrients: World Health Organization.

Andjelković, M., Van Camp, J., De Meulenaer, B., Depaemelaere, G., Socaciu, C., Verloo, M., & Verhe, R. (2006). Iron-chelation properties of phenolic acids bearing catechol and galloyl groups. *Food Chemistry, 98*(1), 23–31. https://doi.org/10.1016/j.foodchem.2005.05.044

Berker, K. I., Güçlü, K., Demirata, B., & Apak, R. (2010). A novel antioxidant assay of ferric reducing capacity measurement using ferrozine as the colour forming complexation reagent. *Analytical Methods, 2*(11), 1770–1778. https://doi.org/10.1039/C0AY00245C

Bertleff-Zieschang, N., Rahim, M. A., Ju, Y.i., Braunger, J. A., Suma, T., Dai, Y., … Caruso, F. (2017). Biofunctional metal-phenolic films from dietary flavonoids. *Chemical Communications, 53*(6), 1068–1071.

Bijlsma, J., de Bruijn, W. J. C., Hageman, J. A., Goos, P., Velikov, K. P., & Vincken, J.-P. (2020). Revealing the main factors and two-way interactions contributing to food discolouration caused by iron-catechol complexation. *Scientific Reports, 10*(1), 8288. https://doi.org/10.1038/s41598-020-65171-1

Dobashi, Y., Hirano, T., Hirano, M., & Ohkatsu, Y. (2008). Antioxidant and photo-antioxidant abilities of catechins. *Journal of Photochemistry and Photobiology A: Chemistry, 197*(2), 141–148. https://doi.org/10.1016/j.jphotochem.2007.12.019

Dowling, S., Regan, F., & Hughes, H. (2010). The characterisation of structural and antioxidant properties of isoflavone metal chelates. *Journal of Inorganic Biochemistry, 104*(10), 1091–1098. https://doi.org/10.1016/j.jinorgbio.2010.06.007

Ejima, H., Richardson, J. J., & Caruso, F. (2017). Metal-phenolic networks as a versatile platform to engineer nanomaterials and biointerfaces. *Nano Today, 12*, 136–148. https://doi.org/10.1016/j.nantod.2016.12.012

El-Sherif, A. A., Shoukry, M. M., & Abd-Elgawad, M. M. A. (2013). Protonation equilibria of some selected α-amino acids in DMSO–water mixture and their Cu(II)-complexes. *Journal of Solution Chemistry, 42*(2), 412–427. https://doi.org/10.1007/s10953-013-9966-0

Elhabiri, M., Carrër, C., Marmolle, F., & Traboulsi, H. (2007). Complexation of iron(III) by catecholate-type polyphenols. *Inorganica Chimica Acta, 360*(1), 353–359. https://doi.org/10.1016/j.ica.2006.07.110

Ferreira, C. M., Pinto, I. S., Soares, E. V., & Soares, H. M. (2015). (Un)suitability of the use of pH buffers in biological, biochemical and environmental studies and their interaction with metal ions–a review. *RSC Advances, 5*(39), 30989–31003. https://doi.org/10.1039/C4RA15453C

Flynn, C. M. (1984). Hydrolysis of inorganic iron(III) salts. *Chemical Reviews, 84*(1), 31–41. https://doi.org/10.1021/cr00059a003

Guo, M., Perez, C., Wei, Y., Rapoza, E., Su, G., Bou-Abdallah, F., & Chasteen, N. (2007). Iron-binding properties of plant phenolics and cranberry's bio-effects. *Dalton Transactions, 43*, 4951–4961. https://doi.org/10.1039/B705136K

Habeych, E., van Kogelenberg, V., Sagalowicz, L., Michel, M., & Galaffu, N. (2016). Strategies to limit colour changes when fortifying food products with iron. *Food Research International, 88*, 122–128. https://doi.org/10.1016/j.foodres.2016.05.017

Hajji, H. E., Nkhili, E., Tomao, V., & Dangles, O. (2006). Interactions of quercetin with iron and copper ions: Complexation and autoxidation. *Free Radical Research, 40*(3), 303–320. https://doi.org/10.1080/10715760500484351

Hider, R. C., Liu, Z. D., & Khodr, H. H. (2001). Metal chelation of polyphenols. *Methods in Enzymology, 335*, 190–203. https://doi.org/10.1016/S0076-6879(01)35243-6

Jovanovic, S. V., Simic, M. G., Steenken, S., & Hara, Y. (1998). Iron complexes of gallocatechins. Antioxidant action or iron regulation? *Journal of the Chemical Society, Perkin Transactions, 2*(11), 2365–2370. https://doi.org/10.1039/A805894F

Kasprzak, M. M., Erxleben, A., & Ochocki, J. (2015). Properties and applications of flavonoid metal complexes. *RSC Advances, 5*(57), 45853–45877. https://doi.org/10.1039/C5RA05069C

Khokhar, S., & Owusu Apenten, R. K. (2003). Iron binding characteristics of phenolic compounds: Some tentative structure-activity relations. *Food Chemistry, 81*(1), 133–140. https://doi.org/10.1016/S0308-8146(02)00394-1

Krabbe, J. G., Lingeman, H., Niessen, W. M. A., & Irth, H. (2005). Screening for metal ligands by liquid chromatography-ligand-exchange-electrospray mass spectrometry. *Journal of Chromatography A, 1093*(1), 36–46. https://doi.org/10.1016/j.chroma.2005.07.022

Lesjak, M., & Srai, S. K. S. (2019). Role of dietary flavonoids in iron homeostasis. *Pharmaceuticals, 12*(3), 119. https://doi.org/10.1093/jn/138.9.1647

Mellican, R. I., Li, J., Mehansho, H., & Nielsen, S. S. (2003). The role of iron and the factors affecting off-color development of polyphenols. *Journal of Agricultural and Food Chemistry, 51*(8), 2304–2316. https://doi.org/10.1021/jf020681c

Mira, L., Tereza Fernandez, M., Santos, M., Rocha, R., Helena Florêncio, M., & Jennings, K. R. (2002). Interactions of flavonoids with iron and copper ions: A mechanism for their antioxidant activity. *Free Radical Research, 36*(11), 1199–1208. https://doi.org/10.1080/1071576021000016463

Mladěnka, P., Macáková, K., Filipský, T., Zatloukalová, L., Jahodář, L., Bovicelli, P., … Saso, L. (2011). In vitro analysis of iron chelating activity of flavonoids. *Journal of Inorganic Biochemistry, 105*(5), 693–701.

Nkhili, E., Loonis, M., Mihai, S., El Hajji, H., & Dangles, O. (2014). Reactivity of food phenols with iron and copper ions: Binding, dioxygen activation and oxidation mechanisms. *Food & Function, 5*(6), 1186–1202. https://doi.org/10.1039/C4FO00007B

Papan, P., Kantapan, J., Sangthong, P., Meepowpan, P., & Dechsupa, N. (2020). Iron (III)-Quercetin Complex: Synthesis, Physicochemical Characterization, and MRI Cell Tracking toward Potential Applications in Regenerative Medicine. Contrast Media & Molecular Imaging, 2020. https://doi.org//10.1155/2020/8877862.

Patel, A. R., Heussen, P. C. M., Hazekamp, J., Drost, E., & Velikov, K. P. (2012). Quercetin loaded biopolymeric colloidal particles prepared by simultaneous precipitation of quercetin with hydrophobic protein in aqueous medium. *Food Chemistry, 133*(2), 423–429. https://doi.org/10.1016/j.foodchem.2012.01.054

Perron, N. R., & Brumaghim, J. L. (2009). A review of the antioxidant mechanisms of polyphenol compounds related to iron binding. *Cell Biochemistry and Biophysics, 53*(2), 75–100. https://doi.org/10.1007/s12013-009-9043-x

Pinelo, M., Manzocco, L., José Nuñez, M., & Cristina Nicoli, M. (2004). Solvent effect on quercetin antioxidant capacity. *Food Chemistry, 88*(2), 201–207. https://doi.org/10.1016/j.foodchem.2004.01.034

Rahim, M. A., Kempe, K., Müllner, M., Ejima, H., Ju, Y.i., van Koeverden, M. P., … Caruso, F. (2015). Surface-confined amorphous films from metal-coordinated simple phenolic ligands. *Chemistry of Materials, 27*(16), 5825–5832. https://doi.org/10.1021/acs.chemmater.5b02790

Reichardt, C., & Welton, T. (2011). *Solvents and solvent effects in organic chemistry*. John Wiley & Sons.

Ren, J., Meng, S., Lekka, C. E., & Kaxiras, E. (2008). Complexation of Flavonoids with Iron: Structure and Optical Signatures. *The Journal of Physical Chemistry B, 112*(6), 1845–1850. https://doi.org/10.1021/jp076881e

Ryan, P., & Hynes, M. J. (2008). The kinetics and mechanisms of the reactions of iron(III) with quercetin and morin. *Journal of Inorganic Biochemistry, 102*(1), 127–136. https://doi.org/10.1016/j.jinorgbio.2007.07.041

Smith, G. J., Thomsen, S. J., Markham, K. R., Andary, C., & Cardon, D. (2000). The photostabilities of naturally occurring 5-hydroxyflavones, flavonols, their glycosides and their aluminium complexes. *Journal of Photochemistry and Photobiology A: Chemistry, 136*(1), 87–91. https://doi.org/10.1016/S1010-6030(00)00320-8

Sokolová, R., Ramešová, Š., Kocábová, J., Kolivoška, V., Degano, I., & Pitzalis, E. (2016). On the difference in decomposition of taxifolin and luteolin vs. fisetin and quercetin in aqueous media. *Monatshefte für Chemie - Chemical Monthly, 147*(8), 1375–1383. https://doi.org/10.1007/s00706-016-1737-3

Stepanic, V., Gasparovic, A. C., Troselj, K. G., Amic, D., & Zarkovic, N. (2015). Selected attributes of polyphenols in targeting oxidative stress in cancer. *Current Topics in Medicinal Chemistry, 15*(5), 496–509. https://doi.org/10.2174/1568026615666150209123100

Stookey, L. L. (1970). Ferrozine: A new spectrophotometric reagent for iron. *Analytical Chemistry, 42*(7), 779–781. https://doi.org/10.1021/ac60289a016

Tan, J., de Bruijn, W. J. C., van Zadelhoff, A., Lin, Z., & Vincken, J.-P. (2020). Browning of epicatechin (EC) and epigallocatechin (EGC) by auto-oxidation. *Journal of Agricultural and Food Chemistry, 68*(47), 13879–13887. https://doi.org/10.1021/acs.jafc.0c0571610.1021/acs.jafc.0c05716.s001

Uivarosi, V., Munteanu, A. C., Sharma, A., & Singh Tuli, H. (2019). Metal Complexation and Patent Studies of Flavonoid. In H. Singh Tuli (Ed.), *Current Aspects of Flavonoids: Their Role in Cancer Treatment* (pp. 39–89). Singapore: Springer Singapore.

Wang, Z. (2013). Iron complex nanoparticles synthesized by eucalyptus leaves. *ACS Sustainable Chemistry & Engineering, 1*(12), 1551–1554. https://doi.org/10.1021/sc400174a

Wienk, K., Marx, J., & Beynen, A. (1999). The concept of iron bioavailability and its assessment. *European Journal of Nutrition, 38*(2), 51–75. https://doi.org/10.1007/s003940050046

Zhong, Q. Z., Li, S., Chen, J., Xie, K., Pan, S., Richardson, J. J., & Caruso, F. (2019). Oxidation-mediated kinetic strategies for engineering metal-phenolic networks. *Angewandte Chemie International Edition, 58*(36), 12563–12568. https://doi.org/10.1002/anie.201907666

Zhou, A., & Sadik, O. A. (2008). Comparative analysis of quercetin oxidation by electrochemical, enzymatic, autoxidation, and free radical generation techniques: A mechanistic study. *Journal of Agricultural and Food Chemistry, 56*(24), 12081–12091. https://doi.org/10.1021/jf802413v